Nonlinear elastic behavior of graphene: *Ab initio* calculations to continuum description

Xiaoding Wei,[1] Benjamin Fragneaud,[1] Chris A. Marianetti,[2] and Jeffrey W. Kysar[1,*]

[1]*Department of Mechanical Engineering, Columbia University, New York, New York 10027, USA*
[2]*Department of Applied Physics and Applied Mathematics, Columbia University, New York, New York 10027, USA*

The nonlinear in-plane elastic properties of graphene are calculated using density-functional theory. A thermodynamically rigorous continuum description of the elastic response is formulated by expanding the elastic strain energy density in a Taylor series in strain truncated after the fifth-order term. Upon accounting for the symmetries of graphene, a total of fourteen nonzero independent elastic constants are determined by least-squares fit to the *ab initio* calculations. The nonlinear continuum description is valid for infinitesimal and finite strains under arbitrary in-plane tensile loading in circumstance for which the bending stiffness can be neglected. The continuum formulation is suitable for incorporation into the finite element method.

I. INTRODUCTION

Recent experiments by Lee *et al.*[1] probed the mechanical properties of graphene by indenting circular free-standing films of monatomic thickness graphene with an atomic force microscope (AFM) until the films ruptured. Graphene films of two diameters (1 and 1.5 μm) were examined with indenter tips of two radii (16.5 and 27.5 nm). The force-displacement response of the indented graphene was nonlinear and insensitive to the diameter of the indenter tip; the nonlinearity was predominantly due to prestrain in the graphene and finite deformation kinematics. The nonlinear elastic behavior of graphene contributed little to the nonlinearity in the force-displacement response because less than about 1% of the graphene film was subjected to strains greater than about 5%, beyond which the nonlinear elastic response initiates. Thus, the force-displacement response of indented graphene films can be assumed to depend upon the linear elastic response, especially at small indentation depths. The force on the indenter at rupture of the graphene films depended upon the radius of the indenter tip, but was insensitive to the diameter of the free-standing film. The distribution of rupture force of the 23 experimentally tested films strongly suggests the graphene films were free of defects. Hence the graphene remained elastic until the film stress reached the intrinsic strength of graphene, at which time rupture occurred. As a consequence, knowledge of the nonlinear elastic properties of graphene is necessary to understand the strength and reliability of structures and devices made of graphene.

Several recent studies[2–5] have probed the nonlinear in-plane elastic response of graphene. Liu *et al.*[2] employed *ab initio* computations to investigate the nonlinear elastic response of both armchair and zigzag nanotubes, and Xiao *et al.*[3] performed molecular dynamics simulations; however neither related the results to a continuum description. Khare *et al.*[4] considered the deformation of graphene in the presence of defects by developing a multiscale model that coupled *ab initio*, molecular dynamics and a linear elastic continuum description via domain decomposition. Lu and Huang[5] simulated the mechanical behavior of graphene under uniaxial deformation to large strains based on an atom-

istic formulation and related the results to a nonlinear continuum formulation. In addition to in-plane deformation of graphene, they also considered the out-of-plane deformation. Recently, Cadelano *et al.*[6] calculated the nonlinear elastic properties of graphene via *ab initio* methods and related the results to a nonlinear elastic description in which the elastic strain energy density is expanded in a Taylor series to include both a quadratic term in strain (which gives rise to a linear elastic response) as well as a cubic term (which allows a softening of the elastic stiffness with strain). In the present study, we also made preliminary efforts to use the same continuum description to describe the results of *ab initio* computations. However, the resulting continuum nonlinear elastic description (with a total of five elastic constants) is unable to capture both the linear response at infinitesimal strain and the maximum stress (i.e., the intrinsic strength) at finite strain with satisfactory fidelity to either experiment or *ab initio* calculations.

In this paper, we adopt a fifth-order series expansion of the strain energy density function in order to model the in-plane elastic properties of graphene and demonstrate that the resulting continuum description (now with fourteen independent elastic constants) describes accompanying *ab initio* results with high accuracy in the infinitesimal strain regime as well as at finite strains, including the strain at the intrinsic stress and beyond. A higher rank tensor is associated with each term of the series expansion and the components of the tensor represent the continuum elastic properties. Previous authors[7–9] had determined the nonzero independent tensor components that correspond to the symmetry elements of graphene for the second-, third-, and fourth-order terms, but not for the fifth-order term. Hence, we also report the independent components of the tenth-rank tensor (for the fifth-order elastic constants) for materials with the symmetries of graphene.

II. FIFTH-ORDER NONLINEAR CONTINUUM ELASTIC DESCRIPTION

Figure 1 shows the graphene atomic unit cell with lattice vectors $\mathbf{a}_1$ and $\mathbf{a}_2$ in the undeformed reference configuration. Upon application of a macroscopically homogeneous defor-
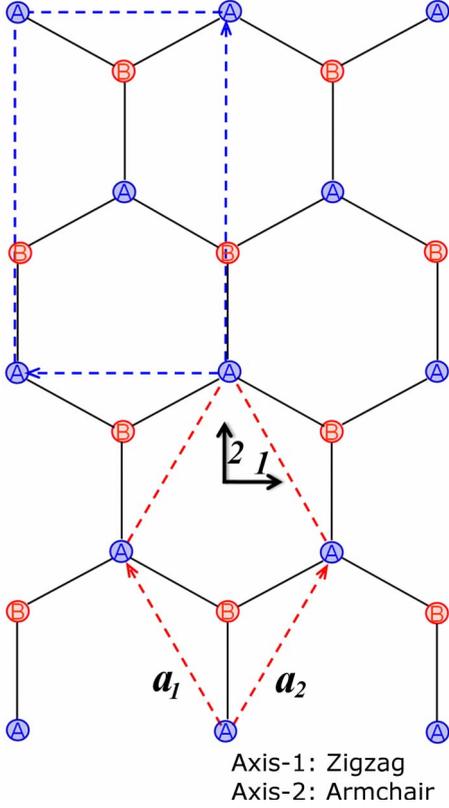
FIG. 1. (Color online) Undeformed graphene lattice, decomposed into sublattice A (blue) and sublattice B (red). Rectangular four-atom unit cell enclosed by blue dashed line and rhomboidal two-atom unit cell enclosed by red dashed line. Zigzag direction coincides with 1-axis and armchair direction coincides with 2-axis.

mation, the lattice vectors of the deformed graphene are $\mathbf{a}'_i = \mathbf{F}\mathbf{a}_i$ (with $i=1,2$), where $\mathbf{F}$ is the deformation gradient tensor. According to the classical Cauchy-Born rule[10] all interior atoms of the unit cell deform according to $\mathbf{F}$ as well; however this rule does not apply to graphene.[11–14] Graphene is represented using two sublattices, A and B, as illustrated in Fig. 1. During deformation, the atom associated with sublattice B in the unit cell adopts a position within the deformed unit cell that minimizes the elastic strain energy density, Φ, of the deformed lattice. Writing the Lagrangian strain $\boldsymbol{\eta} = (1/2)(\mathbf{F}^\mathbf{T}\mathbf{F}-\mathbf{I})$, where $\mathbf{I}$ is the identity tensor, the strain energy density has functional form $\Phi = \Phi(\boldsymbol{\eta})$.

From a continuum perspective, the elastic properties of a material are determined from the elastic strain energy density, Φ, which is quadratic in strain for a linear elastic material. Nonlinear elastic constitutive behavior[15] is established by expanding Φ in a Taylor series in terms of powers of strain, as

$$\Phi = \frac{1}{2!}C_{ijkl}\eta_{ij}\eta_{kl} + \frac{1}{3!}C_{ijklmn}\eta_{ij}\eta_{kl}\eta_{mn}$$

$$+ \frac{1}{4!}C_{ijklmnop}\eta_{ij}\eta_{kl}\eta_{mn}\eta_{op}$$

$$+ \frac{1}{5!}C_{ijklmnopqr}\eta_{ij}\eta_{kl}\eta_{mn}\eta_{op}\eta_{qr} + \cdots, \tag{1}$$

where η_{ij} is Lagrangian elastic strain. Summation convention is employed for repeating indices; lower case subscripts range from 1 to 3. Herein $\mathbf{C}$ denotes each higher-order elastic modulus tensor; the rank of each tensor corresponds to the number of subscripts. The second-order elastic constants (SOEC), C_{ijkl}, third-order elastic constants (TOEC), C_{ijklmn}, fourth-order elastic constants (FOEC), $C_{ijklmnop}$, and fifth-order elastic constants (FFOEC), $C_{ijklmnopqr}$, are given by the components of the fourth-, sixth-, eighth-, and tenth-rank tensors, respectively. The symmetric second Piola-Kirchhoff stress tensor, Σ_{ij}, is

$$\Sigma_{ij} = \frac{\partial\Phi}{\partial\eta_{ij}} = C_{ijkl}\eta_{kl} + \frac{1}{2!}C_{ijklmn}\eta_{kl}\eta_{mn}$$

$$+ \frac{1}{3!}C_{ijklmnop}\eta_{kl}\eta_{mn}\eta_{op} + \frac{1}{4!}C_{ijklmnopqr}\eta_{kl}\eta_{mn}\eta_{op}\eta_{qr}$$

$$+ \cdots. \tag{2}$$

Employing the Voigt[16] notation for subscripts: $11\rightarrow 1$, $22\rightarrow 2$, $33\rightarrow 3$, $23\rightarrow 4$, $31\rightarrow 5$, and $12\rightarrow 6$, (N.B. for strain, $\eta_4=2\eta_{23}$, $\eta_5=2\eta_{31}$, and $\eta_6=2\eta_{12}$), one can rewrite Eqs. (1) and (2) as

$$\Phi = \frac{1}{2!}C_{IJ}\eta_I\eta_J + \frac{1}{3!}C_{IJK}\eta_I\eta_J\eta_K + \frac{1}{4!}C_{IJKL}\eta_I\eta_J\eta_K\eta_L$$

$$+ \frac{1}{5!}C_{IJKLM}\eta_I\eta_J\eta_K\eta_L\eta_M + \cdots, \tag{3}$$

$$\Sigma_I = \frac{\partial\Phi}{\partial\eta_I} = C_{IJ}\eta_J + \frac{1}{2!}C_{IJK}\eta_J\eta_K + \frac{1}{3!}C_{IJKL}\eta_J\eta_K\eta_L$$

$$+ \frac{1}{4!}C_{IJKLM}\eta_J\eta_K\eta_L\eta_M + \cdots, \tag{4}$$

where the summation convention for upper case subscripts runs from 1 to 6. Since Φ is a thermodynamic state function, for a general deformation state the number of the independent components of the SOEC tensor is 21, that of the TOEC tensor is 56, that of the FOEC tensor is 126, and that of the FFOEC tensor is 252 for a material of arbitrary elastic anisotropy.

In this study, we assume that the deformed state of the graphene is such that the contribution of bending to the strain energy density is negligible as compared to the in-plane strain contribution. This requires that the radius of curvature of any out-of-plane deformation be significantly larger than the in-plane interatomic distance. The stress state of graphene under those assumptions can be assumed to be two dimensional (2D), so we need only consider the in-plane stress and strain components. Thus, the only components that need be considered in Eqs. (1) and (2) are those with indices containing exclusively 1 and/or 2. Likewise, only components with subscripts consisting exclusively of 1, 2, and/or 6 need be considered in Eqs. (3) and (4).

Upon accounting for the symmetry of the atomic lattice of graphene, the linear elastic constitutive relationship for the 2D graphene lattice can be expressed as

TABLE I. Higher-order elastic constants (up to the fifth order) of graphene lattice.

SOEC	TOEC	FOEC	FFOEC
C_{11}	C_{111}	C_{1111}	C_{11111}
C_{12}	C_{112}	C_{1112}	C_{11112}
$C_{16}=0$	$C_{116}=0$	$C_{1116}=0$	$C_{11116}=0$
$C_{22}=C_{11}$	$C_{122}=(C_{111}-C_{222}+C_{112})$	C_{1122}	C_{11122}
$C_{26}=0$	$C_{126}=0$	$C_{1126}=0$	$C_{11126}=0$
$C_{66}=\frac{1}{2}$	$C_{166}=\frac{1}{4}$	$C_{1166}=\frac{1}{24}$	$C_{11166}=\frac{1}{40}$
$\times(C_{11}-C_{12})$	$\times(3C_{222}-2C_{111}-C_{112})$	$\times(-5C_{1111}-4C_{1112}+9C_{2222})$	$\times(-4C_{11111}-5C_{11112}+9C_{22222})$
		$C_{1222}=\frac{1}{2}$	$C_{11222}=\frac{1}{2}$
	C_{222}	$\times(C_{1111}+2C_{1112}-C_{2222})$	$\times(C_{11111}+3C_{11112}+2C_{11122}-3C_{12222}-C_{22222})$
	$C_{226}=0$	$C_{1226}=0$	$C_{11226}=0$
	$C_{266}=\frac{1}{4}$	$C_{1266}=\frac{1}{12}$	$C_{11266}=\frac{-1}{120}$
	$\times(2C_{111}-C_{222}-C_{112})$	$\times(C_{1111}+2C_{1112}-3C_{1122})$	$\times(13C_{11111}+30C_{11112}+20C_{11122}-45C_{12222}-18C_{22222})$
	$C_{666}=0$	$C_{1666}=0$	$C_{11666}=0$
		C_{2222}	C_{12222}
		$C_{2226}=0$	$C_{12226}=0$
		$C_{2266}=\frac{1}{24}$	$C_{12266}=\frac{1}{120}$
		$\times(7C_{1111}-4C_{1112}-3C_{2222})$	$\times(8C_{11111}+15C_{11112}-20C_{11122}-3C_{22222})$
		$C_{2666}=0$	$C_{12666}=0$
		$C_{6666}=\frac{1}{16}$	$C_{16666}=\frac{1}{80}$
		$\times(-C_{1111}-8C_{1112}+6C_{1122}+3C_{2222})$	$\times(11C_{11111}+30C_{11112}+10C_{11122}-45C_{12222}-6C_{22222})$
			C_{22222}
			$C_{22226}=0$
			$C_{22266}=\frac{1}{40}$
			$\times(9C_{11111}-5C_{12222}-4C_{22222})$
			$C_{22666}=0$
			$C_{26666}=\frac{1}{80}$
			$\times(-C_{11111}-30C_{11112}+10C_{11122}+15C_{12222}+6C_{22222})$
			$C_{66666}=0$

$$\begin{bmatrix} \Sigma_1 \\ \Sigma_2 \\ \Sigma_6 \end{bmatrix} = \begin{bmatrix} C_{11} & C_{12} & 0 \\ C_{12} & C_{11} & 0 \\ 0 & 0 & \frac{C_{11}-C_{12}}{2} \end{bmatrix} \begin{bmatrix} \eta_1 \\ \eta_2 \\ \eta_6 \end{bmatrix}. \qquad (5)$$

There are only two independent nonzero SOEC components which corresponds to in-plane isotropic linear elasticity[14] for which Young's modulus is $E=(C_{11}^2-C_{12}^2)/C_{11}$ and Poisson's ratio is $\nu=C_{12}/C_{11}$.

Similarly, the components of the TOEC, FOEC, and FFOEC tensors can be determined based on the symmetries of the graphene atomic lattice (point group D_{6h} which consists of a sixfold rotational axis and six mirror planes). Previous studies have shown there to be three independent nonzero in-plane components of the TOEC tensor,[8] and four independent nonzero in-plane components of the FOEC

tensor.[9] For the FFOEC tensor, $C_{ijklmnopqr}$, the lattice symmetry requires

$$C_{abcdefghij} = Q_{ka}Q_{lb}Q_{mc}Q_{nd}Q_{oe}C_{klmnopqrst}Q_{pf}Q_{qg}Q_{rh}Q_{si}Q_{tj}, \qquad (6)$$

where **Q** is the corresponding transformation matrix for each symmetry element. Five independent in-plane components for the FFOEC tensor of graphene result from applying all symmetry operations of the graphene lattice. Table I lists the elastic constants up to fifth order for graphene. With regard to the FOEC components, we chose to designate different independent components than previous authors[9] in order to obtain more compact stress-strain relations, but the relationships between the nonzero components are the same.

The fourteen independent elastic constants of graphene are determined by a least-squares fit to stress-strain results
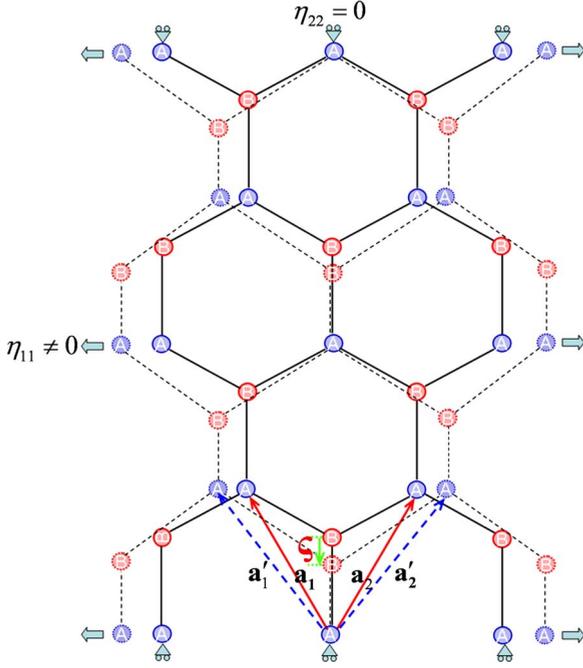
FIG. 2. (Color online) Graphene lattice under uniaxial strain in zigzag direction ($\eta_1 \geq 0$, $\eta_2 = 0$, and $\eta_6 = 0$). Solid circles denote sublattices A and B in undeformed reference configuration. Dashed circles denote sublattices A and B in the deformed configuration. Internal relaxation of sublattice B is denoted by $\mathbf{s}$.

from *ab initio* simulations. Five relationships between stress and strain are necessary because there are five independent FFOECs. We obtain the stress-strain relationships by simulating the following deformation states: uniaxial strain in the zigzag direction (cf. Fig. 2); uniaxial strain in the armchair direction; and, equibiaxial strain. The deformation gradient tensor $\mathbf{F}_{zig}$ for uniaxial strain in the zigzag direction is given as

$$\mathbf{F}_{zig} = \begin{bmatrix} \lambda_1 & 0 \\ 0 & 1 \end{bmatrix}, \tag{7}$$

where λ_1 is the stretch ratio in the zigzag direction. The deformation gradient tensor $\mathbf{F}_{arm}$ for uniaxial strain in the armchair direction is

$$\mathbf{F}_{arm} = \begin{bmatrix} 1 & 0 \\ 0 & \lambda_2 \end{bmatrix}, \tag{8}$$

where λ_2 is the stretch ratio in the armchair direction. The deformation gradient tensor $\mathbf{F}_{bi}$ for equibiaxial strain is

$$\mathbf{F}_{bi} = \begin{bmatrix} \lambda & 0 \\ 0 & \lambda \end{bmatrix}, \tag{9}$$

where λ is the equibiaxial stretch ratio.

From Eq. (4) and Table I, the in-plane stress components (i.e., Σ_1, Σ_2, and Σ_6) for an arbitrary in-plane deformation (η_1, η_2, and η_6) are

$$\Sigma_1 = (C_{11}\eta_1 + C_{12}\eta_2) + \frac{1}{2}\bigg\{ C_{111}\eta_1^2 + (C_{111} - C_{222} + C_{112})\eta_2^2$$

$$+ \left(\frac{3}{4}C_{222} - \frac{1}{2}C_{111} - \frac{1}{4}C_{112}\right)\eta_6^2 + 2C_{112}\eta_1\eta_2 \bigg\}$$

$$+ \frac{1}{6}\bigg\{ C_{1111}\eta_1^3 + \frac{1}{2}(C_{1111} + 2C_{1112} - C_{2222})\eta_2^3$$

$$+ 3C_{1112}\eta_1^2\eta_2 + 3C_{1122}\eta_1\eta_2^2 + \frac{1}{8}(-5C_{1111} - 4C_{1112}$$

$$+ 9C_{2222})\eta_1\eta_6^2 + \frac{1}{4}(C_{1111} + 2C_{1112} - 3C_{1122})\eta_2\eta_6^2 \bigg\}$$

$$+ \frac{1}{24}\bigg\{ C_{11111}\eta_1^4 + C_{12222}\eta_2^4 + \frac{1}{80}(11C_{11111} + 30C_{11112}$$

$$+ 10C_{11122} - 45C_{12222} - 6C_{22222})\eta_6^4 + 4C_{11112}\eta_1^3\eta_2$$

$$+ 2(C_{11111} + 3C_{11112} + 2C_{11122} - 3C_{12222} - C_{22222})\eta_1\eta_2^3$$

$$+ 6C_{11122}\eta_1^2\eta_2^2 + \frac{3}{20}(-4C_{11111} - 5C_{11112} + 9C_{22222})\eta_1^2\eta_6^2$$

$$+ \frac{1}{20}(8C_{11111} + 15C_{11112} - 20C_{11122} - 3C_{22222})\eta_2^2\eta_6^2$$

$$+ \frac{1}{10}(-13C_{11111} - 30C_{11112} - 20C_{11122} + 45C_{12222}$$

$$+ 18C_{22222})\eta_1\eta_2\eta_6^2 \bigg\}, \tag{10}$$

$$\Sigma_2 = (C_{12}\eta_1 + C_{11}\eta_2) + \frac{1}{2}\bigg\{ C_{112}\eta_1^2 + C_{222}\eta_2^2 + \left(\frac{1}{2}C_{111}\right.$$

$$\left. - \frac{1}{4}C_{222} - \frac{1}{4}C_{112}\right)\eta_6^2 + 2(C_{111} - C_{222} + C_{112})\eta_1\eta_2 \bigg\}$$

$$+ \frac{1}{6}\bigg\{ C_{1112}\eta_1^3 + C_{2222}\eta_2^3 + 3C_{1122}\eta_1^2\eta_2 + \frac{3}{2}(C_{1111}$$

$$+ 2C_{1112} - C_{2222})\eta_1\eta_2^2 + \frac{1}{4}(C_{1111} + 2C_{1112}$$

$$- 3C_{1122})\eta_1\eta_6^2 + \frac{1}{8}(7C_{1111} - 4C_{1112} - 3C_{2222})\eta_2\eta_6^2 \bigg\}$$

$$+ \frac{1}{24}\bigg\{ C_{11112}\eta_1^4 + C_{22222}\eta_2^4 + \frac{1}{8}(-C_{11111} - 30C_{11112}$$

$$+ 10C_{11122} + 15C_{12222} + 6C_{22222})\eta_6^4 + 4C_{11122}\eta_1^3\eta_2$$

$$+ 4C_{12222}\eta_1\eta_2^3 + 3(C_{11111} + 3C_{11112} + 2C_{11122} +$$

$$- 3C_{12222} - C_{22222})\eta_1^2\eta_2^2 + \frac{1}{20}(-13C_{11111} - 30C_{11112}$$

$$- 20C_{11122} + 45C_{12222} + 18C_{22222})\eta_1^2\eta_6^2 + \frac{3}{20}(9C_{11111}$$

$$- 5C_{12222} - 4C_{22222})\eta_2^2\eta_6^2 + \frac{1}{10}(8C_{11111} + 15C_{11112}$$

$$- 20C_{11122} - 3C_{22222})\eta_1\eta_2\eta_6^2 \bigg\}, \tag{11}$$

and

$$\Sigma_6 = \frac{C_{11} - C_{12}}{2}\eta_6 + \frac{1}{2}\bigg\{\bigg(\frac{3}{2}C_{222} - C_{111} - \frac{1}{2}C_{112}\bigg)\eta_1\eta_6 + \bigg(C_{111}$$

$$- \frac{1}{2}C_{222} - \frac{1}{2}C_{112}\bigg)\eta_2\eta_6\bigg\} + \frac{1}{6}\bigg\{\frac{1}{16}(-C_{1111} - 8C_{1112}$$

$$+ 6C_{1122} + 3C_{2222})\eta_6^3 + \frac{1}{8}(-5C_{1111} - 4C_{1112}$$

$$+ 9C_{2222})\eta_1^2\eta_6 + \frac{1}{8}(7C_{1111} - 4C_{1112} - 3C_{2222})\eta_2^2\eta_6$$

$$+ \frac{1}{2}(C_{1111} + 2C_{1112} - 3C_{1122})\eta_1\eta_2\eta_6\bigg\}$$

$$+ \frac{1}{24}\bigg\{\frac{1}{10}(-4C_{11111} - 5C_{11112} + 9C_{22222})\eta_1^3\eta_6$$

$$+ \frac{1}{20}(11C_{11111} + 30C_{11112} + 10C_{11122} - 45C_{12222}$$

$$- 6C_{22222})\eta_1\eta_6^3 + \frac{1}{10}(9C_{11111} - 5C_{12222} - 4C_{22222})\eta_2^3\eta_6$$

$$+ \frac{1}{20}(-C_{11111} - 30C_{11112} + 10C_{11122} + 15C_{12222}$$

$$+ 6C_{22222})\eta_2\eta_6^3 + \frac{1}{10}(-13C_{11111} - 30C_{11112} - 20C_{11122}$$

$$+ 45C_{12222} + 18C_{22222})\eta_1^2\eta_2\eta_6 + \frac{1}{10}(8C_{11111} + 15C_{11112}$$

$$- 20C_{11122} - 3C_{22222})\eta_1\eta_2^2\eta_6\bigg\}. \tag{12}$$

For uniaxial strain in the zigzag direction ($\eta_1 \geq 0$, $\eta_2 = 0$, and $\eta_6 = 0$) these expressions reduce to

$$\Sigma_1^{zig} = C_{11}\eta_1 + \frac{1}{2}C_{111}\eta_1^2 + \frac{1}{6}C_{1111}\eta_1^3 + \frac{1}{24}C_{11111}\eta_1^4, \tag{13}$$

$$\Sigma_2^{zig} = C_{12}\eta_1 + \frac{1}{2}C_{112}\eta_1^2 + \frac{1}{6}C_{1112}\eta_1^3 + \frac{1}{24}C_{11112}\eta_1^4, \tag{14}$$

$$\Sigma_6 = 0. \tag{15}$$

For uniaxial strain in the armchair direction ($\eta_1 = 0$, $\eta_2 \geq 0$, and $\eta_6 = 0$) the expressions are

$$\Sigma_1^{arm} = C_{12}\eta_2 + \frac{1}{2}(C_{111} - C_{222} + C_{112})\eta_2^2$$

$$+ \frac{1}{12}(C_{1111} + 2C_{1112} - C_{2222})\eta_2^3 + \frac{1}{24}C_{12222}\eta_2^4, \tag{16}$$

$$\Sigma_2^{arm} = C_{11}\eta_2 + \frac{1}{2}C_{222}\eta_2^2 + \frac{1}{6}C_{2222}\eta_2^3 + \frac{1}{24}C_{22222}\eta_2^4, \tag{17}$$

$$\Sigma_6^{arm} = 0. \tag{18}$$

Finally, for equibiaxial strain ($\eta_1 = \eta_2 = \eta \geq 0$, $\eta_6 = 0$), the stress-strain relationship is

$$\sum_1^{bi} = \sum_2^{bi} = (C_{11} + C_{12})\eta + \frac{1}{2}(2C_{111} - C_{222} + 3C_{112})\eta^2$$

$$+ \frac{1}{6}\bigg(\frac{3}{2}C_{1111} + 4C_{1112} - \frac{1}{2}C_{2222} + 3C_{1122}\bigg)\eta^3$$

$$+ \frac{1}{24}(3C_{11111} + 10C_{11112} - 5C_{12222} + 10C_{11122}$$

$$- 2C_{22222})\eta^4, \tag{19}$$

$$\Sigma_6 = 0. \tag{20}$$

All fourteen elastic constants contribute to the expressions for stress-strain response for these three deformation states.

III. DENSITY-FUNCTIONAL CALCULATIONS

The stress-strain relationship of graphene under the desired deformation configurations is characterized via *ab initio* calculations with the density-functional theory (DFT) code, Vienna *ab initio* simulation package (VASP).[17–20] The generalized gradient approximation is applied by using the revised Perdew-Burke-Ernzerhof functional.[21]

Calculations are performed on both the four-atom graphene unit cell and the two-atom graphene unit cell (Fig. 1); both calculations yield the same results. Here, we focus on the calculation procedure on the two-atom unit cell. The simulation invokes periodic boundary conditions for the two in-plane directions as well as the out-of-plane direction. As such, the simulation assumes the presence of an infinite number of layers of graphene. Thus the height of the unit cell in the out-of-plane axis is maintained at 15 Å which is much larger than the 3.35 Å interlayer spacing of graphite,[22] so the supercell—and hence each layer of graphene—can be treated as isolated. The results of the calculations are independent of the precise value of the out-of-plane thickness, so there is no physical interpretation attached to the quantity. Integration in the Brillouin zone is performed on a $18 \times 18 \times 3$ Gamma centered grid. The kinetic-energy cutoff of the plane wave is set at 800 eV. The calculations are performed at zero temperature.

We first optimize the equilibrium lattice constant for graphene. The total energy as a function of lattice spacing is obtained by specifying several lattice constants varying around 1.412 Å. A least-squares fit of the energy vs lattice constant with a fourth-order polynomial function yields the equilibrium lattice constant, $a_0 = 1.412$ Å, which corresponds to the minimum total energy. The result is within 0.5% of the experimental value of 1.419 Å for graphite.[23]

The strains are imposed by specifying the positions of the atoms of sublattice A on the edges of the unit cell. The positions of the atoms of sublattice B in the plane are not constrained. Therefore, atom *B* in the two-atom unit cell, as shown in Fig. 2, is allowed full freedom of motion within the plane of the graphene lattice. A quasi-Newton algorithm is
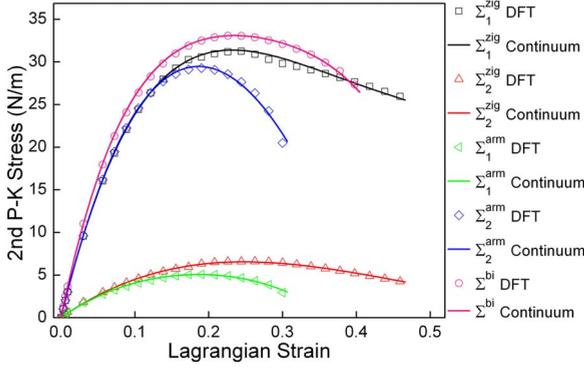
FIG. 3. (Color online) Least-squares fit of stress-strain *ab initio* responses for uniaxial strain in armchair and zigzag directions and equibiaxial strain, where, for example, Σ_1^{arm} indicates the first component in the second P-K stress tensor under uniaxial strain in the armchair direction. The second P-K stress and Lagrangian strain data from *ab initio* calculations are plotted as hollow symbols and least-squares fit results are plotted as solid lines.

used to relax atom *B* into its equilibrium position within the deformed unit cell that yields the minimum total energy for the imposed strain state of the unit cell. Since the calculation of the total energy accounts for the internal relaxation of the sublattice B, it can be expressed as a function of only the macroscopic deformation gradient, i.e., $\Psi = \Psi(\mathbf{F})$, where Ψ is the total energy in the system. The elastic strain energy density is defined as $\Phi = \Psi/V$, where V is the volume of the undeformed supercell.

The DFT calculations confirm there is no internal relaxation of atom *B* within the unit cell when the graphene lattice undergoes equibiaxial strain. This is consistent with isotropic mechanical behavior as required by the continuum expression for equibiaxial deformation state [Eqs. (19) and (20)] and agrees with the results of another study.[14] However, for uniaxial strain in the armchair and zigzag directions, atom *B* does have an internal relaxation, denoted by $\boldsymbol{\varsigma}$ in Fig. 2, along the armchair direction.

The VASP simulation calculates the true or Cauchy stress, $\boldsymbol{\sigma}$, which for graphene must be expressed as a 2D force per length with units of N/m by taking the product of the Cauchy stress (with units of N/m²) and the supercell thickness of 15 Å. The Cauchy stress is related to the second Piola-Kirchhoff (P-K) stress $\boldsymbol{\Sigma}$ as

$$\boldsymbol{\Sigma} = J\mathbf{F}^{-1}\boldsymbol{\sigma}(\mathbf{F}^{-1})^T, \tag{21}$$

where J is the determinant of the deformation gradient tensor $\mathbf{F}$.[24]

IV. DETERMINATION OF CONTINUUM PARAMETERS FROM *AB INITIO* CALCULATIONS

The VASP simulation results, shown in Fig. 3, for the three deformation configurations yield a total of five relationships of the second P-K stress versus Lagrangian strain. The 14 elastic constants of the nonlinear continuum description are determined by a least-squares fit of Eq. (13) through Eq. (19) to the *ab initio* results as illustrated in Fig. 3. The indepen-

TABLE II. Nonzero independent components for the SOEC, TOEC, FOEC, and FFOEC tensor components.

SOEC (N/m)	TOEC (N/m)	FOEC (N/m)	FFOEC (N/m)
$C_{11}^{(2D)}=358.1$	$C_{111}^{(2D)}=-2817$	$C_{1111}^{(2D)}=13416.2$	$C_{11111}^{(2D)}=-31383.8$
$C_{12}^{(2D)}=60.4$	$C_{112}^{(2D)}=-337.1$	$C_{1112}^{(2D)}=759$	$C_{11112}^{(2D)}=-88.4$
	$C_{222}^{(2D)}=-2693.3$	$C_{1122}^{(2D)}=2582.8$	$C_{11122}^{(2D)}=-12960.5$
		$C_{2222}^{(2D)}=10358.9$	$C_{12222}^{(2D)}=-13046.6$
			$C_{22222}^{(2D)}=-33446.7$

dent components of the SOEC, TOEC, FOEC, and FFOEC tensors are listed in Table II. It is of interest to note that the components of the TOEC and FFOEC tensors are all negative, which ensures that the elastic stiffness softens with strain up to that of the intrinsic stress and is negative for larger strains.

Furthermore, from the SOEC in Table II, we obtain the 2D Young's modulus and Poisson's ratio for the graphene lattice as 348 N/m and 0.169, respectively. These values compare well to the elastic modulus and Poisson's ratio of the graphite in the basal plane[25] and also to those reported by Liu *et al.*[2] for graphene.

V. COMPARISON WITH INDEPENDENT *AB INITIO* CALCULATIONS

We now use the higher order elastic continuum description to calculate the stress and deformation state under uniaxial stress, rather than uniaxial strain, in the zigzag and armchair directions and compare to previously published results[2] from *ab initio* simulations. When applying uniaxial stress in the zigzag direction on graphene, the stress and deformation states are $\Sigma_1 \geq 0$, $\Sigma_2 = \Sigma_6 = 0$, $\eta_1 \geq 0$, $\eta_2 \leq 0$, and $\eta_6 = 0$ for which Eqs. (10) and (11) reduce to

$$
\begin{aligned}
\Sigma_1 = {} & (C_{11}\eta_1 + C_{12}\eta_2) + \frac{1}{2}\{C_{111}\eta_1^2 + (C_{111} - C_{222} + C_{112})\eta_2^2 \\
& + 2C_{112}\eta_1\eta_2\} + \frac{1}{6}\Big\{C_{1111}\eta_1^3 + \frac{1}{2}(C_{1111} + 2C_{1112} \\
& - C_{2222})\eta_2^3 + 3C_{1112}\eta_1^2\eta_2 + 3C_{1122}\eta_1\eta_2^2\Big\} + \frac{1}{24}\{C_{11111}\eta_1^4 \\
& + C_{12222}\eta_2^4 + 4C_{11112}\eta_1^3\eta_2 + 2(C_{11111} + 3C_{11112} + 2C_{11122} \\
& - 3C_{12222} - C_{22222})\eta_1\eta_2^3 + 6C_{11122}\eta_1^2\eta_2^2\}
\end{aligned} \tag{22}
$$

and

$$
\begin{aligned}
\Sigma_2 = {} & (C_{12}\eta_1 + C_{11}\eta_2) + \frac{1}{2}\{C_{112}\eta_1^2 + C_{222}\eta_2^2 + 2(C_{111} - C_{222} \\
& + C_{112})\eta_1\eta_2\} + \frac{1}{6}\Big\{C_{1112}\eta_1^3 + C_{2222}\eta_2^3 + 3C_{1122}\eta_1^2\eta_2 \\
& + \frac{3}{2}(C_{1111} + 2C_{1112} - C_{2222})\eta_1\eta_2^2\Big\} + \frac{1}{24}\{C_{11112}\eta_1^4
\end{aligned}
$$

$$+ C_{22222}\eta_2^4 + 4C_{11122}\eta_1^3\eta_2 + 4C_{12222}\eta_1\eta_2^3 + 3(C_{11111}$$
$$+ 3C_{11112} + 2C_{11122} - 3C_{12222} - C_{22222})\eta_1^2\eta_2^2\} = 0. \quad (23)$$

Similarly, for graphene under uniaxial tension in the armchair direction, the stress and deformation states are $\Sigma_2 \geq 0$, $\Sigma_1 = \Sigma_6 = 0$, $\eta_1 \leq 0$, $\eta_2 \geq 0$, and $\eta_6 = 0$ whereupon Eqs. (10) and (11) reduce to

$$\Sigma_1 = (C_{11}\eta_1 + C_{12}\eta_2) + \frac{1}{2}\{C_{111}\eta_1^2 + (C_{111} - C_{222} + C_{112})\eta_2^2$$

$$+ 2C_{112}\eta_1\eta_2\} + \frac{1}{6}\left\{C_{1111}\eta_1^3 + \frac{1}{2}(C_{1111} + 2C_{1112}\right.$$

$$\left. - C_{2222})\eta_2^3 + 3C_{1112}\eta_1^2\eta_2 + 3C_{1122}\eta_1\eta_2^2\right\} + \frac{1}{24}\{C_{11111}\eta_1^4$$

$$+ C_{12222}\eta_2^4 + 4C_{11112}\eta_1^3\eta_2 + 2(C_{11111} + 3C_{11112} + 2C_{11122}$$

$$- 3C_{12222} - C_{22222})\eta_1\eta_2^3 + 6C_{11122}\eta_1^2\eta_2^2\} = 0 \quad (24)$$

and

$$\Sigma_2 = (C_{12}\eta_1 + C_{11}\eta_2) + \frac{1}{2}\{C_{112}\eta_1^2 + C_{222}\eta_2^2 + 2(C_{111} - C_{222}$$

$$+ C_{112})\eta_1\eta_2\} + \frac{1}{6}\left\{C_{1112}\eta_1^3 + C_{2222}\eta_2^3 + 3C_{1122}\eta_1^2\eta_2\right.$$

$$\left. + \frac{3}{2}(C_{1111} + 2C_{1112} - C_{2222})\eta_1\eta_2^2\right\} + \frac{1}{24}\{C_{11112}\eta_1^4$$

$$+ C_{22222}\eta_2^4 + 4C_{11122}\eta_1^3\eta_2 + 4C_{12222}\eta_1\eta_2^3 + 3(C_{11111}$$

$$+ 3C_{11112} + 2C_{11122} - 3C_{12222} - C_{22222})\eta_1^2\eta_2^2\}. \quad (25)$$

The stress-strain response for graphene under uniaxial tension in the zigzag and armchair directions is obtained, respectively, by numerically solving Eqs. (22) and (23) as well as Eqs. (24) and (25). The results are shown in Fig. 4(a) expressed in terms of nominal stress and strain and in Fig. 4(b) expressed in terms of second P-K stress and Lagrangian strain. The *ab initio* calculation results reported by Liu *et al.*[2] for graphene under the same conditions are included for comparison.[26] A very good correspondence exists between the two independent calculations, even for strains as large as 30%. The results demonstrate that the conventional definition of Poisson's ratio breaks down under large deformation since it becomes a function of strain. The maximum Cauchy stress for graphene under uniaxial stress in the zigzag direction predicted by our nonlinear elastic constitutive model is 39.5 N/m compared with 40.5 N/m reported by Liu *et al.*[2]

VI. CONCLUSIONS

In conclusion, we developed a multiscale model to characterize the in-plane nonlinear elastic properties of graphene which spans from the atomic length scale to the continuum scale. The continuum description has 14 elastic constants. It accurately describes the linear-elastic behavior at infinitesi-
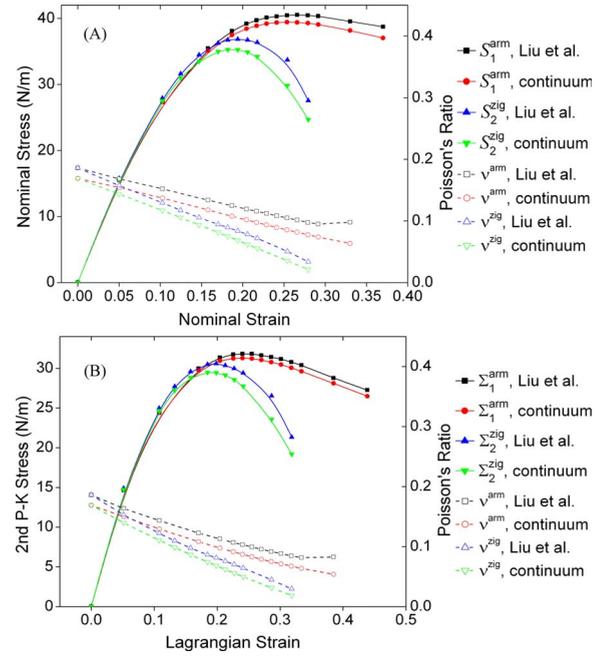
FIG. 4. (Color online) Comparison of the stress-strain relationship (solid symbols) and Poisson's ratio (open symbols) for graphene under uniaxial stress in the armchair and zigzag directions predicted by the nonlinear continuum formulation with that from the calculations reported by Liu *et al.* (Ref. 2). Superscripts represent direction in the graphene in which the uniaxial stress is applied and the subscripts represent stress components. Also ν^{arm} denotes the ratio $-\eta_2/\eta_1$ for graphene under uniaxial tension in the armchair direction. (a) Stress-strain response expressed in nominal stress denoted by S and nominal strain; (b) stress-strain response expressed in second P-K stress and Lagrangian strain.

mal strain and it captures the intrinsic strength (also called the theoretical strength). The graphene lattice is unstable and would rupture spontaneously at strains larger than that which corresponds to the intrinsic strength. Nonlinear behavior initiates at about 5% strain and the elastic behavior becomes noticeably anisotropic at strains about 15%. The formulation is valid for deformation states for which the contribution of bending to the strain energy density is negligible as compared to in-plane deformation (i.e., where the radius of curvature of the deformed graphene is significantly larger than the in-plane interatomic lattice spacing). Hence, this elastic constitutive formulation is not appropriate for use in circumstance for which buckling may occur. The continuum constitutive relations are ideally suited for the finite element method.

*Author to whom correspondence should be addressed; jk2079@columbia.edu

[1] C. Lee, X. Wei, J. Kysar, and J. Hone, Science **321**, 385 (2008).

[2] F. Liu, P. Ming, and J. Li, Phys. Rev. B **76**, 064120 (2007).

[3] T. Xiao, X. J. Xu, and K. Liao, J. Appl. Phys. **95**, 8145 (2004).

[4] R. Khare, S. Mielke, J. Paci, S. Zhang, R. Ballarini, G. Schatz, and T. Belytschko, Phys. Rev. B **75**, 075412 (2007).

[5] Q. Lu and R. Huang, J. Appl. Mech. **1**, 443 (2009).

[6] E. Cadelano, P. L. Palla, S. Giordano, and L. Colombo, Phys. Rev. Lett. **102**, 235502 (2009).

[7] H. Huntington, *The Elastic Constants of Crystals* (Academic, New York, 1964).

[8] F. G. Fumi, Phys. Rev. **86**, 561 (1952).

[9] T. S. G. Krishnamurty, Acta Crystallogr. **16**, 839 (1963).

[10] M. Born and K. Huang, *Dynamical Theory of Crystal Lattices* (Oxford University Press, New York, 1998).

[11] P. Zhang, Y. Huang, P. H. Geubelle, P. A. Klein, and K. C. Hwang, Int. J. Solids Struct. **39**, 3893 (2002).

[12] M. Arroyo and T. Belytschko, J. Mech. Phys. Solids **50**, 1941 (2002).

[13] H. Jiang, P. Zhang, B. Liu, Y. Huang, P. Geubelle, H. Gao, and K. Hwang, Comput. Mater. Sci. **28**, 429 (2003).

[14] J. Zhou and R. Huang, J. Mech. Phys. Solids **56**, 1609 (2008).

[15] R. A. Toupin and B. Bernstein, J. Acoust. Soc. Am. **33**, 216 (1961).

[16] J. F. Nye, *Physical Properties of Crystals* (Oxford Science Publications, Oxford, 1985), pp. 134–135.

[17] G. Kresse and J. Hafner, Phys. Rev. B **49**, 14251 (1994).

[18] G. Kresse and J. Hafner, Phys. Rev. B **48**, 13115 (1993).

[19] G. Kresse and J. Furthmüller, Phys. Rev. B **54**, 11169 (1996).

[20] G. Kresse and J. Furthmüller, Comput. Mater. Sci. **6**, 15 (1996).

[21] B. Hammer, L. Hansen, and J. Norskov, Phys. Rev. B **59**, 7413 (1999).

[22] R. Al-jishi and G. Dresselhaus, Phys. Rev. B **26**, 4514 (1982).

[23] Y. Baskin and L. Meyer, Phys. Rev. **100**, 544 (1955).

[24] M. Crisfield, *Non-Linear Finite Element Analysis of Solids and Structures* (John Wiley & Sons, New York, 1991), pp. 18–19.

[25] O. L. Blakslee, J. Appl. Phys. **41**, 3373 (1970).

[26] A potential for confusion exists in the notation. The graphene lattice has armchair and zigzag directions as in Fig. 1. By convention, an armchair nanotube has the armchair graphene direction oriented around its circumference with the zigzag graphene direction parallel to its axis, and vice versa for a zigzag nanotube. Liu *et al.* (Ref. 2) report their results for graphene under uniaxial stress with the nanotube convention, rather than the graphene convention. For consistency, we report their results using the graphene convention.